# Comparative Analysis of Computational Mesh Cost and Accuracy for Conformal and Nonconformal Meshing in HTGR Lower Plenum

Moon Hyeok Kang, Jeong Ik Lee\*

Dept. Nuclear & Quantum Eng., KAIST, 291 Daehak-ro, Yuseong-Gu, Daejeon 34141, Republic of Korea \*Corresponding author: <u>jeongiklee@kaist.ac.kr</u>

\*Keywords: High Temperature Gas-cooled Reactor, Lower Plenum, Computational Fluid Dynamics

### 1. Introduction

The conceptual design of high-temperature gas-cooled reactors (HTGRs) in Korea requires large-scale three-dimensional CFD analyses, and the computational cost becomes prohibitively expensive when turbulence, heat transfer, and real-gas effects are all taken into account. Multiple international organizations participate in OECD/NEA HTGR benchmarking activities that use experimental data from the Oregon State University (OSU) High Temperature Test Facility (HTTF) to develop CFD workflows for the HTGR lower plenum [1][2]. The HTTF lower plenum is the region where jets from numerous coolant channels exiting the core blocks and mix before merging into the outlet nozzle ("hot duct"); it contains flow-distribution elements and multiple graphite support posts.

The complex geometry promotes shear-layer development and flow separation/reattachment, and recirculation. These jet—mixing—turning characteristics hinder symmetry-based mesh reduction and straightforward domain simplification.

To clarify terminology, conformal (CF) mesh is defined as a single, topologically continuous grid in which neighboring cells share matching faces across all subregions; fluxes are evaluated on common controlvolume faces without interpolation. In contrast, a nonconformal (NC) mesh comprises independently generated subdomain grids whose non-matching faces are coupled through interface conditions that transfer mass, momentum, and energy in a conservative manner. CF typically provides sharper resolution of gradients across subregion boundaries but can be harder to generate for intricate, multi-feature geometries because local refinements propagate globally. NC allows each subdomain to use a mesh best suited to its local physics and length scales, often reducing overall cell count and memory while introducing limited interpolation across interfaces.

In ANSYS CFX, NC connectivity is realized via non-matching interfaces (e.g., General Grid Interface) with "conservative flux transfer" option enabled, which computes surface-to-surface overlap and applies area-weighted flux mapping so that globally conserved quantities remain balanced across the interface. This capability underpins the present comparison: CF versus NC on the same HTTF lower-plenum configuration, under identical physics and numerics, to quantify the cost–accuracy trade.

The purpose of this study is to systematically compare the cost-accuracy balance between CF and nonconformal meshing on the same HTTF lower-plenum domain. Under a steady RANS (k– $\omega$  SST) setup in ANSYS CFX, this study evaluated (i) the predictive accuracy and grid-convergence behavior of global metrics—pressure drop ( $\Delta P$ ) and average outlet velocity and temperature—(ii) the fidelity of local flow structures near the hot duct and in the outer mixing region, and (iii) cell-count metrics, both quantitatively and qualitatively. The results show that NC can be advantageous for large-scale, system-level CFD studies, whereas CF—or a hybrid approach—may be preferred when local phenomena are of primary interest.

## 2. Methodology

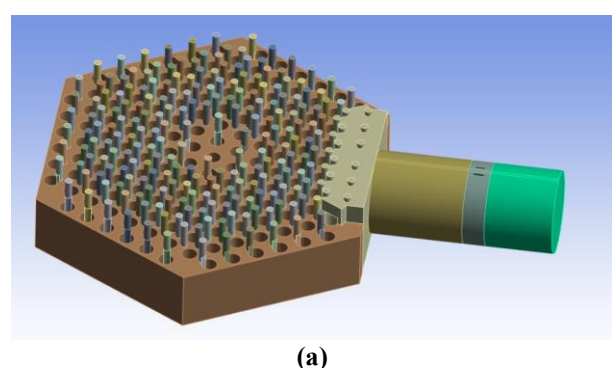
This study divides the HTTF lower plenum into functional subdomains and applies two meshing approaches—CF and NC—to each, respectively (Fig. 1). The CF approach uses a single, conformally connected mesh, whereas the NC approach employs independently meshed subdomains coupled through interfaces with conservative flux correction. For both approaches, three spatial resolutions (coarse, medium, and fine) were generated to assess grid sensitivity. The outlet static pressure was fixed at 0.8 MPa, and walls were treated as adiabatic, no-slip; inlet conditions followed the benchmark specifications (Appendix).

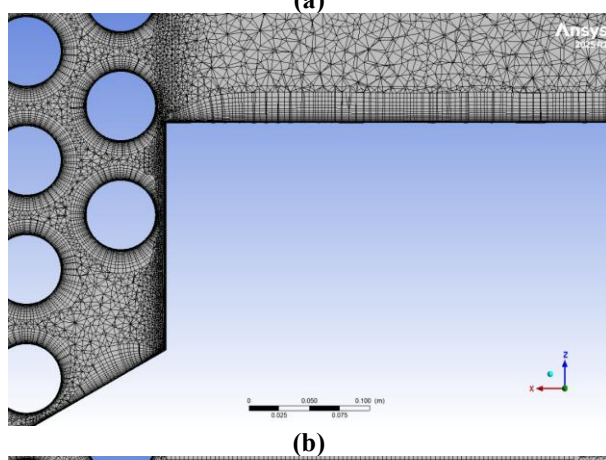
For CF meshing strategy, a single, contiguous volume mesh was generated so that all region boundaries share matching faces. Near-wall layers (inflation) were applied on walls, posts, and the hot-duct surfaces to keep the mean y<sup>+</sup> in the viscous sublayer. Local refinements were placed around jet impingement, separation, and turning zones; because of conformity, these refinements propagate into adjacent regions to maintain face matching. This construction avoids interface interpolation and preserves sharp cross-regional gradients at the discrete level.

For NC meshing strategy and interface placement, each functional subdomain (e.g., outer mixing region, post array, hot-duct approach, and outlet) was meshed independently with locally appropriate element types and refinements, including near-wall inflation to maintain comparable y<sup>+</sup> targets. Subdomains were connected using nonconformal interfaces with conservative flux transfer. The conservative interface ensures mass, momentum, and energy balance across non-matching grids via area—based flux mapping, enabling system-level accuracy with fewer cells.

Simulations were performed in ANSYS CFX 25R2 with the k– $\omega$  SST turbulence model in a steady RANS framework, using high-order discretization for the convective and turbulence terms. The near-wall mesh was refined so that the mean  $y^+$  lies within the viscous

sublayer, improving the reliability of the pressure-drop prediction. As global metrics, the inlet—outlet pressure drop and the average outlet velocity and temperature were used; as local metrics, this study examined separation, reattachment, and shear-layer development near the hot duct and in the outer mixing region to compare the predictive performance of CF and NC.





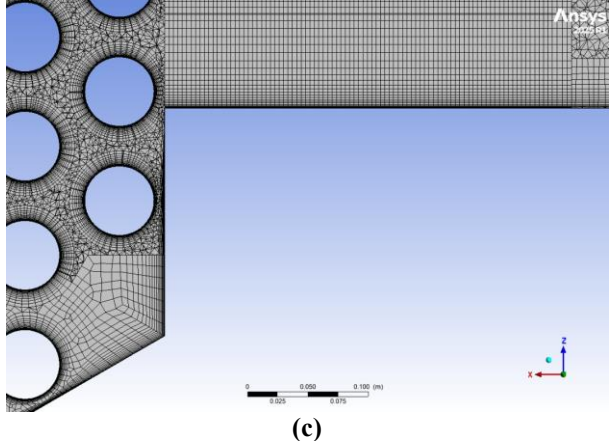


Fig. 1. HTTF lower-plenum simulation domain with CF/NC mesh comparison: (a) domain decomposition, (b) CF mesh resolution near walls and support posts, (c) NC non-matching connectivity example

## 3. Results

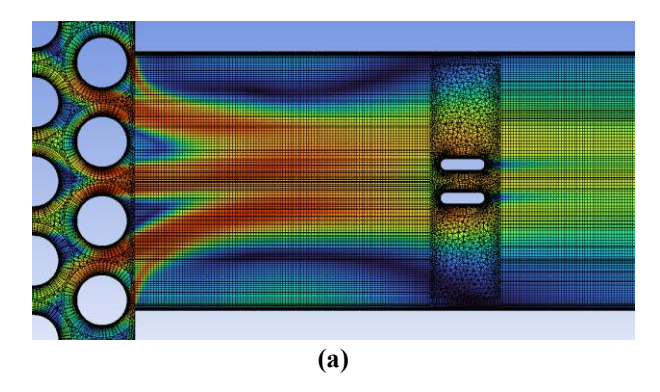
From the simulations, both CF and NC exhibited improved asymptotic behavior as the grid resolution increased, and the two approaches showed similar predictive trends for pressure drop and for the average outlet velocity and temperature (Table 1). This indicates that, when a conservative interface is employed, the NC approach can achieve sufficient accuracy for globally conserved quantities.

Table 1. Key metrics for each case (CF, NC)

CF	Coarse	Medium	Fine
Cell #	44.4M	62.6M	90.5M
$y_{mean}^+$	2.41	1.61	1.46
$\Delta P_{avg}$ (kPa)	1.15	1.20	1.20
$\left  ec{V}  ight _{avg}$ (m/s)	33.5	33.6	33.6
$T_{avg}$ (K)	900	900	900
NC	Coarse	Medium	Fine
NC Cell #	Coarse 27.3M	Medium 39.2M	Fine 64.8M
Cell#	27.3M	39.2M	64.8M
Cell #  y^+_mean	27.3M 3.32	39.2M 2.48	64.8M 2.21

While Fig. 2 shows that CF resolves separation/reattachment and shear-layer development more sharply, these local differences did not translate into large changes in the global metrics over the operating range considered. Therefore, for design workflows primarily driven by system-level losses and bulk outlet conditions, detailed resolution of local structures is of secondary importance; NC is adequate for global loss prediction.

From a cost perspective, NC substantially reduces cell count, memory usage, and solve time, enabling broad parametric sweeps and efficient coupling with system-level tools. NC can serve as a practical baseline for design and system-level assessments, with CF applied selectively when specific local criteria (e.g., peak wall temperature or erosion risk) are explicitly required.



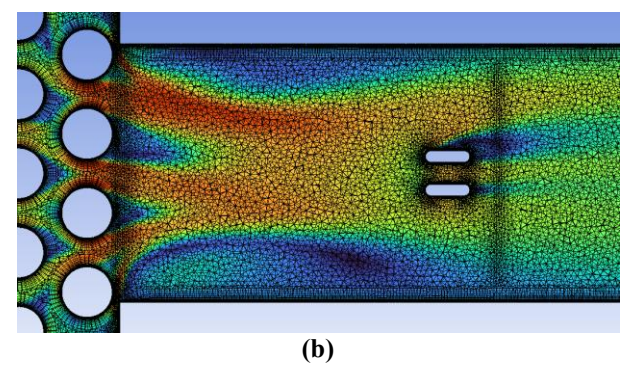


Fig. 2. Comparison of local velocity distribution: (a) NC-mesh case (b) CF-mesh case

## 4. Conclusions

In the comparative study of the HTTF lower plenum, the NC mesh provided sufficient accuracy for global metrics across the operating range examined, whereas the CF mesh captured local separation, reattachment, and shear-layer development more sharply. The high local fidelity of CF did not, however, yield material changes in global metrics within this range. Given its lower cell count, memory footprint, and computing time, NC is recommended as the default option for design workflows oriented toward system-level behavior and integration with system tools. CF is best reserved for cases in which local quantities of interest—such as peak wall temperature, near-wall stress, mixing hot spots, or erosion risk—govern requirements or margins.

Future work should delineate the validity limits of NC, quantify and mitigate numerical and physical stability issues observed in some NC cases, and formalize practical criteria that balance accuracy against mesh-cost constraints. Extensions should also include configurations with conjugate heat transfer, unsteady jet mixing, and real-gas effects.

## **ACKNOWLEDGEMENT**

This work was supported by the National Research Foundation of Korea(NRF) grant funded by the Korea government (MSIT) (No. RS-2024-00457356).

The authors thank Aaron Epiney and Izabela Gutowska for coordinating the benchmark and providing the necessary materials.

We would like to acknowledge the technical support from ANSYS Korea.

### REFERENCE

[1] Hua, Thanh, Jun Fang, and Ling Zou. HTTF Benchmarking Activities in FY 2023. No. ANL/NSE-23/55. Argonne National Laboratory (ANL), Argonne, IL (United States), 2023.

[2] Halsted, Joshua, and Izabela Gutowska.
"Verification and validation of a lower plenum mixing test at the OSU High Temperature Test Facility."
Nuclear Engineering and Design 406 (2023): 112251.

# APPENDIX

Zone ID	Velocity (m/s)	Temperature (K)
CG0	30.389	984.34
CG-1A	23.513	924.658
CG-2A	25.709	889.08
CG-3A	26.618	944.901
CG-4A	26.405	926.654
CG-5A	21.83	866.424
CG-1B	23.513	925.415
CG-2B	25.69	890.425
CG-3B	26.61	947.609
CG-4B	26.446	932.229
CG-5B	21.828	867.567
CG-1C	23.511	924.788
CG-2C	25.702	889.276
CG-3C	26.608	945.155
CG-4C	26.394	926.902
CG-5C	21.825	866.606
CG-1D	23.52	922.995
CG-2D	25.794	886.395
CG-3D	26.772	941.098
CG-4D	26.586	922.794
CG-5D	21.91	863.558
CG-1E	23.517	920.054
CG-2E	25.9	881.331
CG-3E	27.101	932.826
CG-4E	27.129	913.384
CG-5E	22.303	856.71
CG-1F	23.521	922.956
CG-2F	25.796	886.341
CG-3F	26.775	941.027
CG-4F	26.589	922.725
CG-5F	21.911	863.508
Outer bypass	20.669	810.051
	L	1